



Journal of Advanced Research in Fluid Mechanics and Thermal Sciences

Journal homepage:
https://semarakilmu.com.my/journals/index.php/fluid_mechanics_thermal_sciences/index
ISSN: 2289-7879



Effects of Different Phase Change Material Arrangement on Thermal Management for Lithium-Ion Batteries

Vignesh Veeresparan¹, Harish Rajan^{1,*}

¹ School of Mechanical Engineering, Vellore Institute of Technology, Chennai, Tamil Nadu 600127, India

ARTICLE INFO

Article history:

Received 13 December 2022
Received in revised form 2 March 2023
Accepted 10 March 2023
Available online 24 March 2023

Keywords:

Phase change material; lithium-ion batteries; liquid fraction; CFD; trans-radial arrangement

ABSTRACT

The high energy density, low self-discharge, and operating voltages of lithium-ion batteries make them the preferred choice for electric cars. It is crucial to keep the battery pack at operational temperatures in order to avoid thermal runaways because these high energies are being stored in a small area. In this research, a novel passive battery cooling method is presented that makes use of two different phase change materials (PCM) arranged in various ways inside a battery pack. In this study, RT50 and RT60 PCMs are utilized to evaluate the combined thermal performance to that of a single PCM. A variety of configurations for the phase change material are used between battery pack cells, including trans-axial, trans-radial arrangements and compared against the performance of individual PCM. The effectiveness of passive cooling is evaluated in the current study for a variety of layouts that are exposed to external convection circumstances at a constant ambient temperature of 25°C. The transient behaviour of the battery cell temperature and its effects on PCM architecture at various melting stages are investigated in the current work. The heat transmission characteristics and melting phenomenon to suggested phase change materials arrangements is assessed.

1. Introduction

Climate change has emerged as one of the major environmental issues of recent years. Governments are concentrating more on cleaner and leaner energy to address this issue and lower GHG (Greenhouse Gas) emissions as indicated by Panchal *et al.*, [1]. Due to this, the automotive industry was subject to strict restrictions requiring HEV (Hybrid Electric Vehicle) and EV (Electric Vehicle) adaptation in order to dramatically cut emissions. A lithium-ion battery is a crucial component of any HEV or EV system, powering it throughout various driving cycles. As a result, maintaining the system in ideal operating conditions is necessary for a longer product life cycle. The advantages of lithium-ion batteries include their high energy, high power, and longer life. Rapid charging, high load capacity, and low self-discharge are other features. Li-ion batteries are therefore more promising than conventional batteries as a result. Li-ion batteries are utilized in EVs due to their

* Corresponding author.

E-mail address: harish.r@vit.ac.in

<https://doi.org/10.37934/arfmts.104.2.5164>

safety, affordability, longevity, and low temperature performance. Chen *et al.*, [2] suggests the Li-ion batteries to stand out among the batteries used in EVs and HEVs due to their superior performance, high specific energy, low self-discharge, low maintenance requirements, extended cycle life, lightweight nature, and flexible design. Batteries typically exhibit unsatisfactory thermal behavior and an uneven temperature distribution under severe operation conditions. This could lead to a thermal runaway or a degradation in performance and lifetime. Numerous studies have demonstrated that as temperature rises, the electrolyte's conductivity also rises. Therefore, in this case, a high temperature would enable more current to flow through it, which would result in the thermal runaway event.

Various coolant techniques, including air, liquid, and PCM, can be utilized for thermal management of batteries. Kumar *et al.*, [3] investigation found that for battery settings involving a high ambient temperature and a rapid discharge rate, air cooling is insufficient. According to research by Kim *et al.*, [4], Low energy density batteries can be maintained with passive cooling, however high energy density batteries need active cooling. Due to its high specific heat, thermal conductivity, and high heat transfer coefficient, liquid cooling is seen to be a better thermal management alternative than an air-based cooling system as indicated by Han *et al.*, [5]. Despite these advantages, the liquid cooling approach has a number of drawbacks because of system design, extra weight from the coolant flow pump, high maintenance requirements, and expensive setup costs. Kumar *et al.*, [3] identified that liquid cooling systems have security problems, such as coolant leaks that might result in short circuiting incidents or battery thermal failure. Limitations of air and liquid cooling, such as high ambient temperature, additional components, high maintenance, and cost, can be overcome with PCM-based cooling. The large latent heat energy storage of PCM makes it possible to absorb additional energy during phase change without any temperature increase as indicated by Keshteli *et al.*, [6]. On the other hand, Wang *et al.*, [7] puts forth PCM's drawbacks as lower thermal conductivity (as low as 0.2 W/m.K), may interfere with the charging-discharging process during the phase change period.

Solid-liquid PCM is initially in its solid state, it behaves as a sensible storage material and absorbs heat as the temperature rises. Once it hits the melting point, PCM starts to behave like a latent heat material until the phase shifts completely to liquid. Huge amounts of heat are absorbed during this phase transition, which keeps the temperature constant until the transformation is complete. PCM resumes its sensible storage material behavior when it becomes liquid. Al-Hallaj and Selman *et al.*, [8] first employed the concept of lower battery temperature and maintain temperature uniformity by usage of PCM. Bais *et al.*, [9] numerically investigated for a single PCM around battery for varying thickness and concluded that minimum of 4mm PCM thickness is required for effective battery temperature control. Another numerical investigation is performed by Choudhari *et al.*, [10] in a battery pack by using PCM and fin structures. It was found that fin arrangement provided at the interior batteries resulted in better thermal performance. Moraga *et al.*, [11] compared one- and three-layer arrangement of different PCM and discovered that decahydrate sodium carbonate and three-layer arrangements had lower temperatures (eicosane, capric acid, decahydrate sodium carbonate and octadecane). According to Naeshi *et al.*, [12], a three-layer PCM architecture surrounding batteries works best when a PCM with a higher thermal conductivity is placed near to the battery. The layout also has the benefit of lowering temperature by exposing external walls to natural convection. Jilte *et al.*, [13] have compared single layered PCM around the battery cell and multi-layered PCM in both the radial and axial directions have demonstrated decreased cell temperature.

The primary goal of the current study is to ascertain the impact of high discharge rate RT50 and RT60 melting and thermal characteristics on 18650 Li-Ion battery cells. To further investigate the

melting and temperature of the battery, several configurations including trans-radial and trans-axial designs are numerically examined. Each configuration is accessed for its thermal behavior of PCM with respect to its position inside its thermal management enclosure. Several thermal characteristics like liquid fraction, battery temperature and heat transfer coefficients were examined when used in multiple combinations among the configurations.

2. Methodology

Figure 1(a) depicts the schematic of the baseline arrangement using a single 18,650 battery enclosed by a PCM. To represent the battery heating mechanism, a dummy 18,650 battery cell is positioned in the center of an insulated cylindrical container. The battery measures 18 mm in diameter and 65 mm in height, and its center is equipped with an electrical cylindrical heater measuring 6.35 mm (1/4 inch) in diameter and 40 mm in length. The PCM-containing cylindrical container is thought to be thermally insulated and has an inner diameter of 15 mm. The PCMs RT-50 and RT-60 utilized in this work have melting points of 47°C to 51°C and 55°C to 61°C, respectively. Tables 1 and 2 show the thermophysical characteristics of PCMs, respectively. It is assumed that the PCM is initially in the solid state and that the initial and ambient temperatures are both 25°C. A typical 18,650 battery may produce 9.2W of heat at greater discharge rates of 10C, according to research by Yang *et al.*, [14]. In order to replicate battery heating at these high discharge rates, a constant heat generation of 8.8W is required.

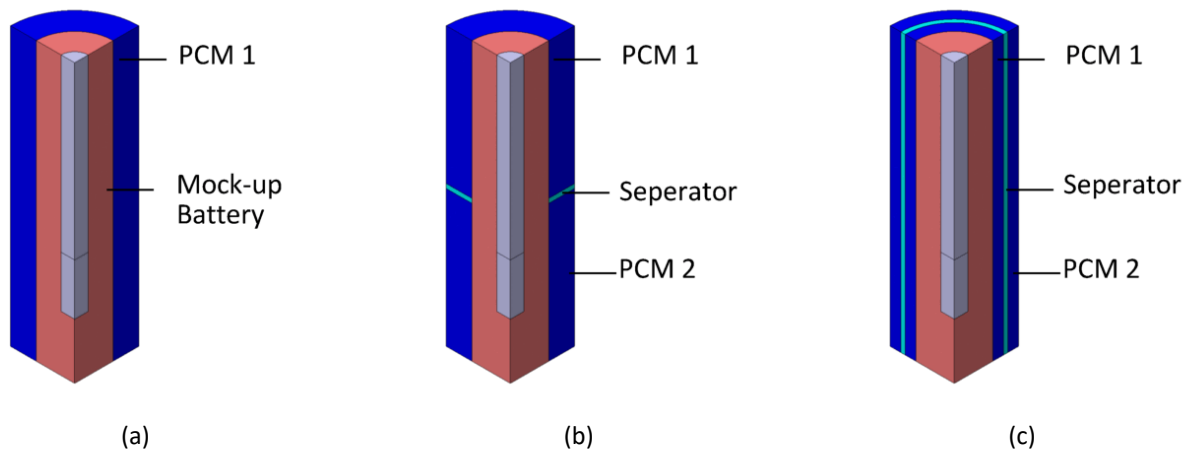


Fig. 1. The geometrical model used in the present study (a) the baseline arrangement; (b) Trans-Axial arrangement; (c) Trans-Radial Arrangement of PCM inside an adiabatic enclosure

Table 1

Thermo-physical parameters of PCM materials

	Density (kg/m ³)	Specific heat (J/Kg.K)	Latent heat (J/Kg)	Solidus Temperature (°C)	Liquidus Temperature (°C)	Viscosity (Kg/(m.s))	Thermal Expansion Coefficient(1/K)	Thermal Conductivity (W/m.K)
RT 50	880	2000	160000	45	51	0.01	0.00091	0.2
RT 60	880	2000	160000	55	61	0.01	0.00091	0.2

Table 2
 Thermo-Physical parameters of other materials [16]

	Density (Kg/m ³)	Thermal Conductivity (W/m.K)	Specific Heat (J/Kg.K)
Aluminum	2719	155	871
Battery	2510	39.96	1028
Heater	7930	16	500

A two-dimensional model with a single cell thickness is constructed for the numerical analysis due to the symmetry of the model and flow behavior. To simulate the generation of heat from batteries, the constant heat source is applied to the cylindrical heater. The battery and PCM's outside walls are considered as thermally insulated. The PCM's numerical modeling is assumed on the following conditions as proposed by Hao *et al.*, Rao *et al.*, and Javani *et al.*, [15,17-18].

- i. Thermophysical characteristics of PCM Materials are assumed to be constant
- ii. PCM material at liquid state are considered to be incompressible Newtonian fluid [19-22]
- iii. The density variations are taken into account using Boussinesq's approximation
- iv. Radiation effects are regarded as insignificant [23,34]

The governing equations used are

Continuity Equation

$$\frac{\partial \rho}{\partial t} + \nabla \cdot (\rho \vec{V}) = 0 \quad (1)$$

Momentum Equation

$$\rho \frac{\partial \vec{V}}{\partial t} + \rho (\vec{V} \cdot \nabla) \vec{V} = -\nabla P + \mu \nabla^2 \vec{V} + \rho \beta \vec{g} (T - T_{Ref}) + \vec{S} \quad (2)$$

Energy Equation

$$\frac{\partial (\rho H)}{\partial t} + \nabla \cdot (\rho \vec{V} H) = \nabla \cdot (k \nabla T) \quad (3)$$

where, ρ is the density of liquid PCM, \vec{V} is the velocity vector components of the liquid PCM, P is the pressure, μ is the dynamic viscosity of the liquid PCM, T is the temperature of PCM, T_{Ref} is the reference temperature, \vec{S} is the momentum source of the liquid PCM, k is the thermal conductivity of the PCM and \vec{g} is the gravity vector. The problem of phase change material melting is modelled using the enthalpy-porosity approach and calculated as formulated by Ling *et al.*, [25]. The liquid portion of the phase change materials represents both the solid and liquid phases, and the enthalpy H is therefore given as

$$H = h_{ref} + \int_{T_{Ref}}^T C_{PCM} dT + \gamma L \quad (4)$$

where, h_{ref} is the reference enthalpy, L is the latent heat of PCM. The following equation is used to compute the liquid fraction γ ,

$$\gamma = \begin{cases} 0, & \text{if } T < T_s \\ 1, & \text{if } T > T_l \\ \frac{T-T_l}{T_l-T_s}, & \text{if } T_s \leq T \leq T_l \end{cases} \quad (5)$$

where, T_s is the solidus melting temperature of PCM, T_l is the liquidus melting temperature of PCM. This represents that PCM is in solid state when $\gamma=0$, and in liquid state when $\gamma=1$. The region between 0 and 1 is known as mushy zone.

The ANSYS Fluent commercial fluid flow solver is used for solving the governing equations. The melting characteristics are captured by creating a uniformly structured grid. The ambient temperature of 25°C and at this temperature PCM remains in its solid state is used as the initial conditions to simulate this physics. The cylindrical enclosure with PCM material is assumed to be at completely adiabatic in nature. Hence, the cylindrical enclosure is not modeled and exterior face of the PCM is assigned to be adiabatic wall condition. The PISO algorithm is used to couple the equations for pressure and momentum. The quantities solved are discretized using a second order upwind method. For pressure corrections, the PRESTO scheme is employed. For the convergence, the under-relaxation factors default values are utilized. For continuity, momentum, and energy, the residuals are set to 1×10^{-6} and 1×10^{-9} , respectively [26]. After 100 inner iterations, the convergence requirements were satisfied. For this investigation, 0.1s of time step and quad cells with a 0.25mm size are employed. The simulation required the full power of the workstation for around one day to fully resolve the melting problem.

The prior numerical analysis serves to validate the used correlations and numerical methodology. The melting of paraffin wax inside an aluminum enclosure was substantiated by Yang *et al.*, [14] numerical simulation. The Figure 2(a) presents numerical data for PCM liquid fraction over time with an 8.8W battery heat. PCM remains to be in solid state until 200 seconds to receive heat from battery as sensible heat. Thereafter, the PCM starts to melt and stores the heat from battery as latent heat to reduce the battery temperature.

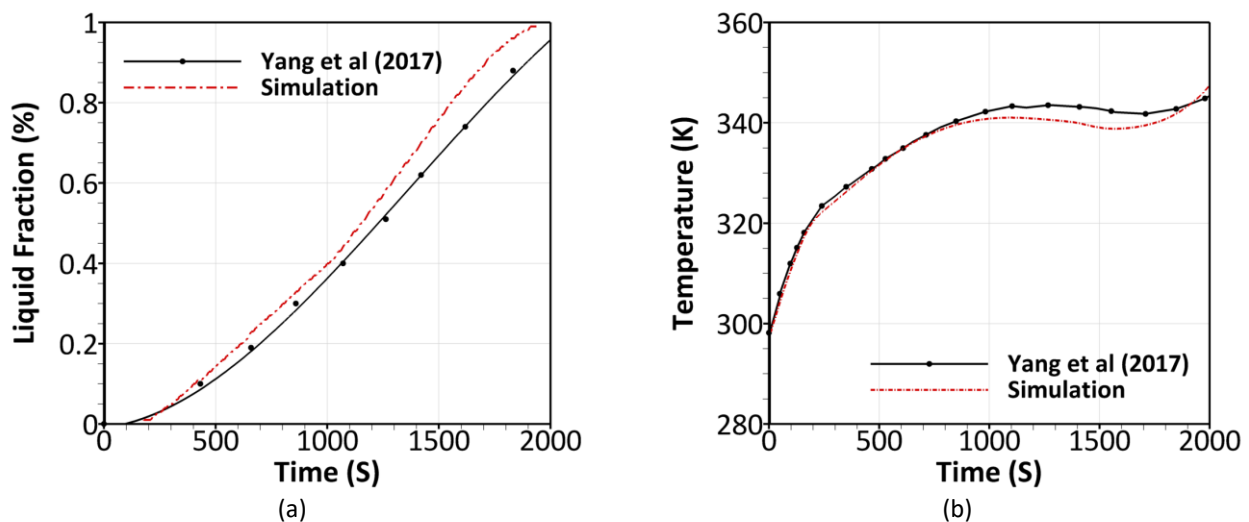


Fig. 2. (a) The variation of liquid fraction in present study and simulation of Yang *et al.*, [12] (b) The variation of battery temperature in the present study and simulation of Yang *et al.*, [12]

At the end of 2000 seconds, the PCM is completely melted and starts to store the heat as sensible heat. The Figure 3 shows that the liquid fraction contours of the current investigation and those of

the prior numerical analysis are in within 10% error and captures the melting trend in good accord. The Figure 2(b) represents the numerical data of battery temperature over time with 8.8W of battery heat. Until 200 seconds, the temperature increases steeply up to 51°C and then it reduces the level of temperature increase until 1000 seconds to 71°C. The temperature almost remains constant up to 2000 seconds and then increases steeply to 87°C at the end of 2500 seconds. The battery temperature of the current investigation is closely matching at the initial half of the time period and then there is an error of 4% for the rest of the time period studied. Both the liquid fraction and battery temperature are in good agreement with the prior numerical work.

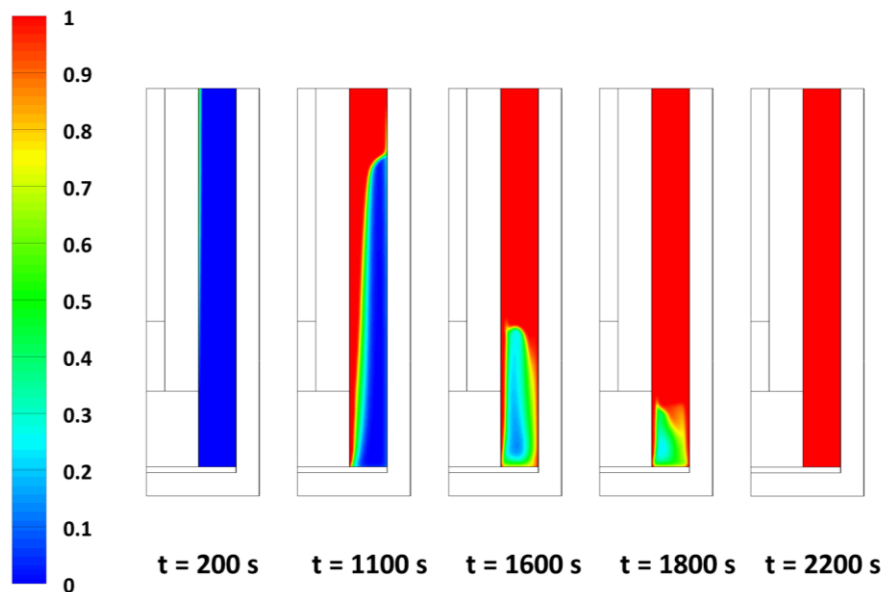


Fig. 3. Validation of the Liquid fraction contours at various time in the present study

3. Results

3.1 Comparison of RT50 and RT60 PCM Performance

To enable the use of PCM passive cooling technology for battery thermal management, it is crucial to estimate the thermal properties. Under a constant ambient temperature of 25°C, the two different phase change materials behave differently when the battery heats. It is allowed for the battery to discharge at its maximum rate of 8.8W. Since the PCM's external surfaces are considered to be adiabatic, there shouldn't theoretically be any heat transfer here. Heat is produced by the heater inside the battery, and it is transferred to the PCM. At the end of 150 seconds, RT50 PCM begins to melt, and at the end of 250 seconds, RT60 PCM begins to melt. RT50 PCM melts half of its volume after 600 seconds, while RT60 PCM melts half of its volume after 710 seconds. RT50 melts entirely in 1150 seconds, while RT60 takes 1270 seconds to melt completely. Due to lower solidus and liquidus melting temperatures, as seen in Figure 4(a), RT 50 melts 6% quicker than RT60. The average battery temperature is progressively rising due to the continuous heat from the battery. The PCM in the RT50 arrangement continues to receive sensible heat when the battery temperature rises to its 45°C melting point. After that, it keeps receiving heat while operating in latent heat storage mode until it reaches 67°C. Figure 4(b) demonstrates that, after 800 seconds, the PCM entirely returns to sensible heat and loses its ability to store latent heat. Similar to this, the RT60 configuration continues to absorb heat in the form of latent heat storage up to 77°C before shifting back to sensible heat at the end of 800 seconds when it reaches its melting point of 55°C.

The temperature plateau was not primarily noticeable due of the high discharge rates from battery. Figure 4(a) and (b) illustrates that after 200 seconds, RT50 has begun to melt along the battery's sidewalls whereas RT60 is still solid. After 600 seconds, the PCM that is closer to the walls has increased melting volume and has delayed the battery temperature increase. This continuous until the PCM melts totally and loses its capacity to store latent heat. The lower latent heat and high melting temperature of the phase change materials are really the primary causes of the absence of a temperature plateau. This investigation shows that RT60 PCM has nearly 13% delay to completely melt the PCM compared to RT50 PCM. Also, the battery temperature at PCMs peak melting point have maximum of 10% higher than RT50 PCM. This comparative investigation demonstrates that phase transition materials with a lower melting point and comparable latent heat capacity could temporarily keep the battery at lower temperatures. In contrast, phase transition materials with greater melting temperatures and comparable latent heat capacities may resist higher temperatures for a longer period of time, which is above the functioning limits of batteries.

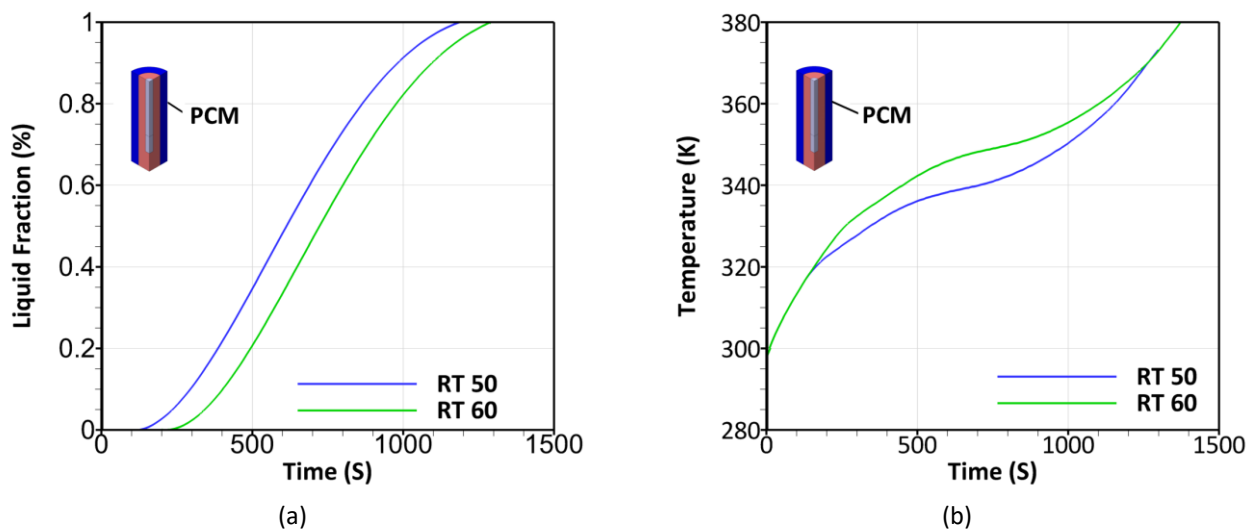


Fig. 4. (a) Effect of single layer PCM on the liquid fraction; (b) Effect of single layer PCM on the battery temperature

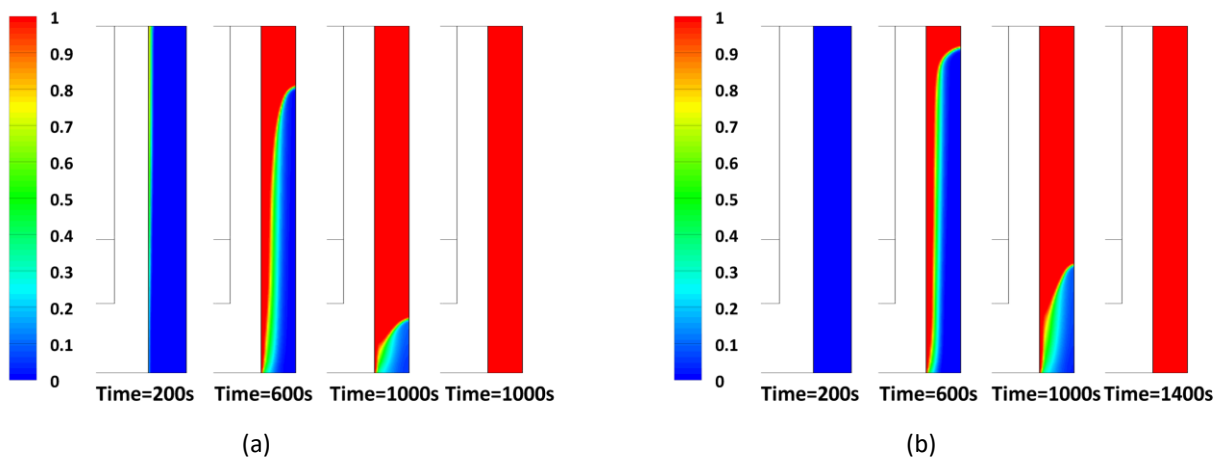


Fig. 5. (a) Liquid fraction contour for RT50 PCM; (b) Liquid fraction contour for RT60 PCM

3.2 Comparison of Trans-Axial Arrangements

As covered in the prior section, the two different PCM materials each offer advantages and disadvantages depending on their respective melting temperatures. The goal of this research is to comprehend how these two materials behave when placed in trans-axial configurations and separated by an aluminum separator. To improve heat transfer from the battery to the PCM, an aluminum separator is used. For this investigation, there were two trans-axial arrangements: TA60-50 and TA50-60. In a TA60-50 configuration, the RT60 is located on the upper half of the battery while the RT50 is located on the lower half. Similar to the TA50-60 layout, RT50 is positioned higher while RT60 is positioned lower. The battery is enclosed in an adiabatic enclosure of PCM materials, similar to the prior work. The upper part of the mock-up battery receives the majority of the heat produced by the heater, which is located inside the battery. While the battery's lower half experiences significantly less heat than its upper half. In order to enhance the latent heat capacity of phase change materials, melting occurs in the upper half of the material and, as a result of the buoyancy effect, the liquid moves from bottom to top. The melting fraction of the PCM remains the same in both trans-axial setups between 200 and 600 seconds, respectively. This is because the separator serves as a heat dissipator from the battery to the PCM. However, with time, the RT50 PCM on the upper part of the TA50-60 arrangement experiences more heat and cools more quickly than it does in the TA60-50 configuration. Figure 6 (a) demonstrates that until 800 seconds into the RT50 melting phase, the battery temperature stays between 57°C and 62°C. The temperature of the battery starts to gradually rise as RT50 approaches the conclusion of the latent heat storage and reaches 107°C after 1400 seconds. The placement of RT60 in the upper half of the battery in TA60-50 configurations allowed heat to be directed to the lower half of the PCM, which has a lower melting temperature. Lower melting temperature of the PCM in the lower half and greater melting temperature in the upper half will cause the higher heat to be directed from the upper half to lower half as the lower PCM hits the melting temperature since the lower half receives less heat than the upper half. However, in the TA50-60 configuration, the RT50 positioned at the upper half receives the majority of the heat due to the lower melting temperature, and the RT60 positioned at the lower half receives a significantly lower amount of heat due to the effect of the higher melting temperature of the RT60. The battery temperature would be maintained between 57°C and 77°C for 650 seconds in the TA60-50 configuration shown in Figure 6(b). While the TA50-60 configuration could only sustain a temperature range of 57°C to 62°C for a shorter time.

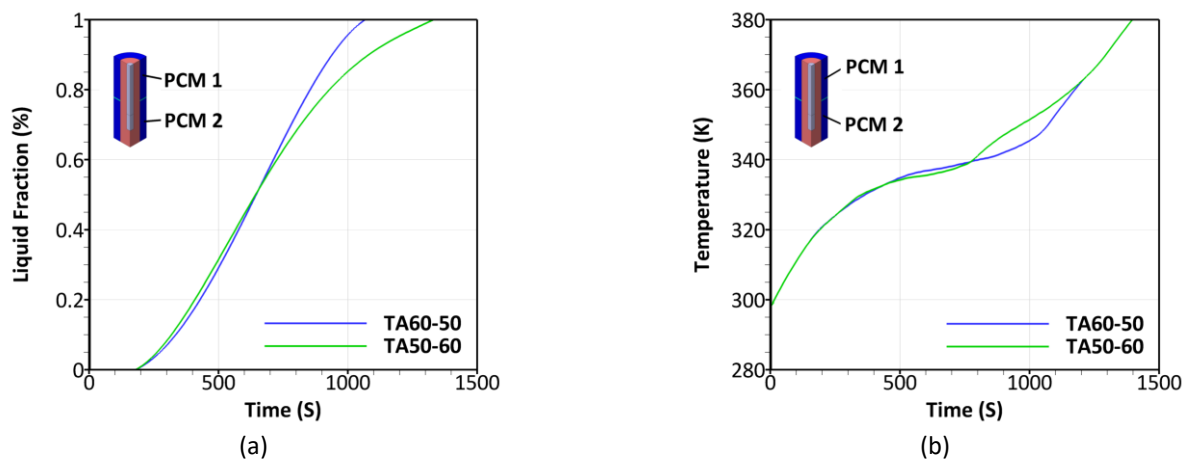


Fig. 6. (a) Effect of Trans-axial PCM on the liquid fraction; (b) Effect of Trans-axial PCM on the battery temperature

Figure 7(a) and (b) illustrates that by the end of 200 seconds, the RT50 in both trans-axial arrangements had begun to melt. The RT60 positioned in the top half of the battery tends to melt at a slower rate and the RT50 placed in the lower half of the battery tends to melt at a faster rate as the melting progresses due to the battery heat at 600 seconds. The PCM in the top half feels heat coming from three directions, while the PCM in the bottom half feels heat coming from only two directions. As a result, we could see that the PCM, which is positioned in the upper half, is melting at the bottom, side, and top. Heat is transferred through the sidewalls and separator at PCM in the lower half. TA60-50 configurations, regardless of their melting temperatures, exhibit equal volume fractions after 1000 seconds. This demonstrates that the phase change material in this configuration has reached a state of thermal equilibrium. This investigation shows that TA60-50 & TA50-60 PCM configurations were nearly same up to 800 seconds for liquid fraction and battery temperature. After which the TA50-60 configuration takes nearly 20% more time to completely melt the PCM compared to TA60-50. Also, the battery temperature at PCMs peak melting point in TA60-50 configurations have maximum of 10% higher than TA50-60 PCM configurations. This indicates unambiguously that the PCM's trans-axial location has a major impact on battery temperature.

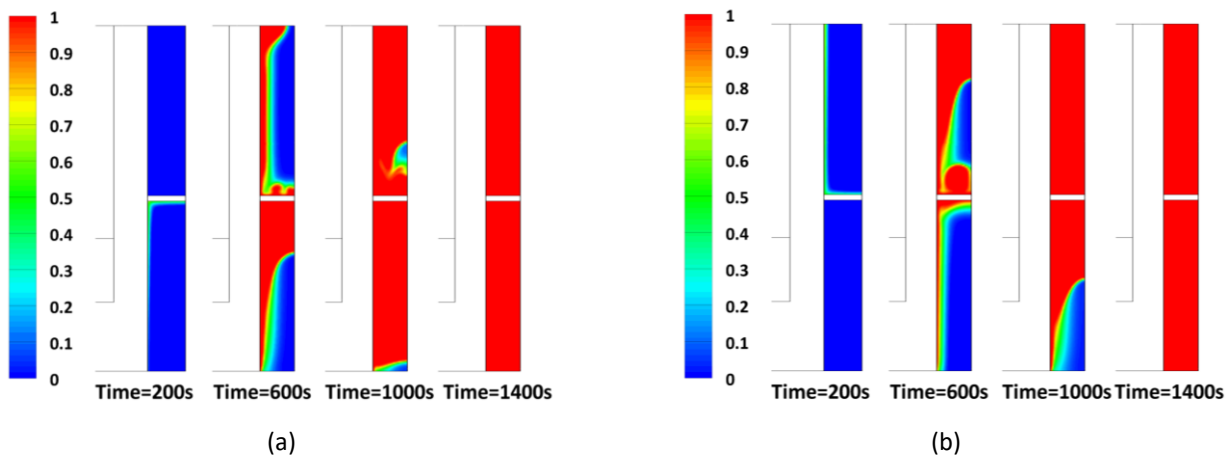


Fig. 7. (a) Liquid fraction contour for TA60-50 arrangement; (b) Liquid fraction contour for TA50-60 arrangement

3.3 Comparison of Trans-Radial Arrangements

To understand better its thermal behavior in terms of battery temperature and PCM melt fraction, the two distinct PCM materials used in this work are arranged in radial directions. Two distinct PCM separated by an aluminum separator are studied for two trans-radial arrangements. To improve the heat transfer between the battery and PCMs, a TR60-50 arrangement with RT60 filled in the inner cylinder and RT50 at the outside cylinder was first used. The TR50-60 configuration begins to melt at the end of 150 seconds of heat generation from the battery, and the TR60-50 configuration begins to melt at the end of 250 seconds. In the inner layer of the TR50-60 arrangement, as shown in Figure 8(a), RT50 begins to absorb heat and stores it as latent heat for up to 550 seconds before regaining its sensible heat and storing the heat. By improving the heat transfer from RT50 to RT60, the aluminum separator enables RT60 to store the heat as latent heat. This is evident from the graph, which shows how the liquid fraction curve abruptly changed at 550 seconds. Until the end of 1100 seconds, the latent heat storage of heat is active. After that, the RT60 loses its ability to store latent heat. In the TR60-50 setup, Figure 8(b) illustrates that the RT60 PCM begins to melt at the start of

250 seconds and continues to have a smooth increase in the PCM liquid percentage over the course of 700 seconds. It takes longer for this design to melt until it reaches 40% of the liquid PCM. After then, PCM melts more quickly under the combined impacts of RT60 and RT50 than under the TR50-60 arrangement. For both designs, the battery's initial temperature rises continuously until it reaches its melting point. For TR50-60, the PCM begins to absorb heat as latent heat as soon as the temperature reaches 45°C, whereas for TR60-50, it takes a temperature of 55°C to do so. The change from latent to sensible heat causes a dramatic increase in heat flow at the conclusion of the inner layer's complete melting in the TR50-60 arrangement. As a result, the exterior layer of the battery still has RT60, which will absorb heat and lower the battery's temperature. The double slope curve is clearly shown in the figure, with the lower slope representing the inner layer PCM's behavior and the top slope representing the outer layer PCM's behavior. PCM reaches the sensible heat storage after completely melting in both layers, which causes a constant rise in temperature.

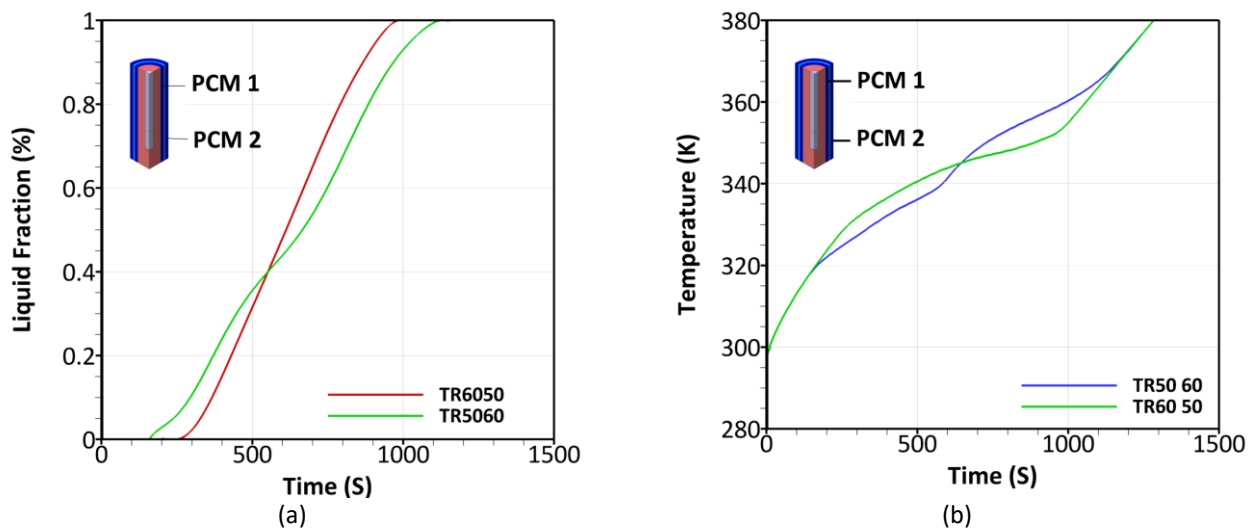


Fig. 8. (a) Effect of Trans-radial PCM on the liquid fraction; (b) Effect of Trans-radial PCM on the battery temperature

The inner layer RT60, on the other hand, starts to absorb heat as latent heat from the beginning of the 61°C and continues to do so until the temperature reaches 72°C in TR60-50 configurations. The second slope further reduces the temperature growth rate up to 1000 seconds after melting starts at RT50 to absorb the extra heat from RT60. The temperature in the TR50-60 setup is lower between 200 and 600 seconds and higher between 600 and 1100 seconds. Figure 9(a) and (b), however, illustrates how the TR60-50 arrangement has a lower temperature rate than the TR50-60 setup. Even though the latter design offered a faster time, the battery working temperature was not maintained.

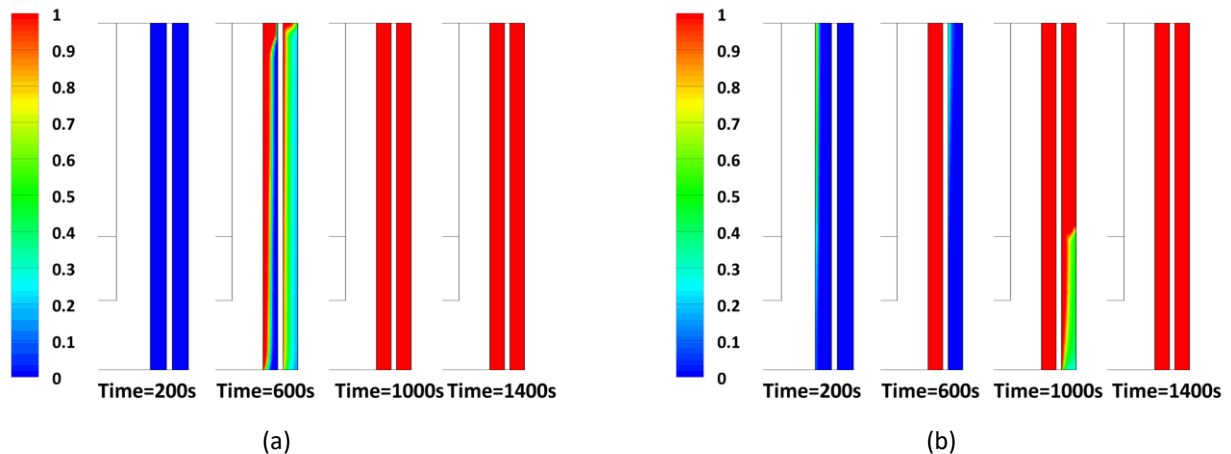


Fig. 9. (a) Liquid fraction contour for TA60-50 arrangement; (b) Liquid fraction contour for TA50-60 arrangement

This investigation shows that TR50-60 PCM configuration started to melt early by 150 seconds and melted completely by 1100 seconds. Though TR60-50 PCM configurations shows that melting starts by 200 seconds and melts PCM complete by 1000 seconds. This shows TR60-50 configuration is 10% faster compared to TR50-60 configurations in terms of complete melting of PCM. Also, initially up to 600 seconds the battery temperature was low in TR50-60 but after that TR60-50 configuration shows better temperature management in battery. On average, TR60-50 configuration is 7% better than TR50-60 configurations in terms of battery temperature. The location of the PCM in the radial arrangement and its effects on thermal behaviour are also made evident in this work.

3.4 Comparison of Heat Transfer Coefficients within the Arrangements

To understand convective heat transfer in the suggested designs, a comparison study between various PCM arrangements and configurations was undertaken. Figure 10(a) demonstrates that when melting starts in PCM, RT50 and RT60 quickly achieve their highest heat transfer coefficients of 52 W/m².K and 44 W/m².K, respectively. Due to the earlier melting point in RT50 compared to RT60, the heat transfer coefficient was greater. Because melting occurs at lower temperatures, PCM transforms from a solid to a liquid and, due to the buoyancy effect, draws heat away from the battery. In terms of a single PCM, the RT50 performs better in terms of long- term, greater heat transfer coefficients. Due to the stacking of lower melting PCM above and higher melting PCM below, the maximum heat transfer coefficient in the TA50-60 configuration is 42 W/m².K, which is lower than the TA60-50 configuration. Figure 10(b) demonstrates that after it reaches its maximum heat transfer coefficients, the delivery of 40 W/m².K remains constant for 200 seconds to 700 seconds. The greatest heat transfer coefficient in the TA60-50 arrangement, however, was 44 W/m².K at the end of 150 seconds, and it then gradually decreased until it reached 25 W/m².K at 800 seconds. Heat transfer coefficient increases for 100 seconds while the RT60 at the bottom of the battery is melting to its maximum. The heat transfer coefficient gradually decreases once peak melting is complete.

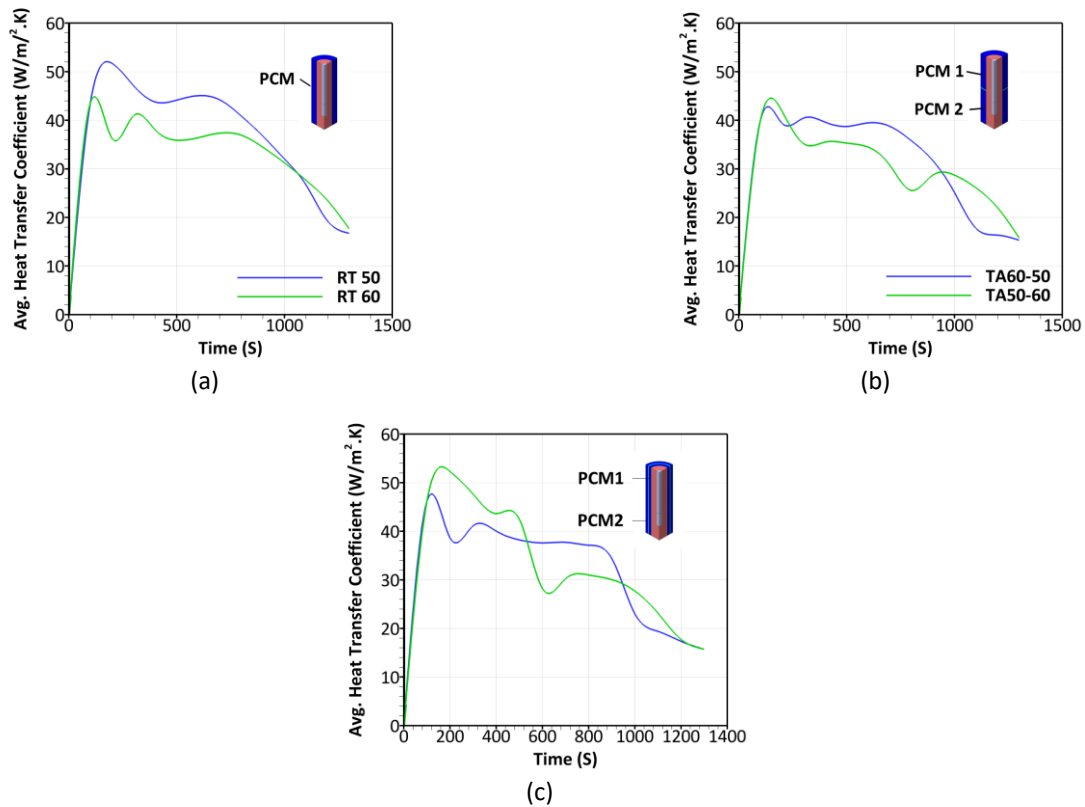


Fig. 10. (a) Effect of heat transfer coefficient for single layer arrangement; (b) Effect of heat transfer coefficient for Trans-axial arrangement; (c) Effect of heat transfer coefficient for Trans-radial arrangement

When arranged in a trans-radial fashion, TR50–60 reaches its maximum heat transfer coefficient of 52 W/m².K, then steadily reduces the up to 28 W/m².K, increases once again due to the peak melting of RT60, and steadily decreases the up to 18 W/m².K. As shown in Figure 11(c), the heat transfer coefficient in the TR60-50 arrangement gradually decreases to a maximum of 38 W/m².K, then slowly decreases to 18 W/m².K after the PCM has completely melted. For single layer arrangement at its peak melting point, the average heat transfer coefficient of RT50 PCM is 26% higher than RT60 PCM arrangement. For Trans axial arrangement at its peak melting point, the average heat transfer coefficient of TA60-50 configuration is 16% higher than TA50-60 configurations. For Trans-radial case, TR60-50 configuration shows 12% lower up to 600 seconds and after that it increases to 26% at end of 1000 seconds when compared against TR50-60 configuration. This indicates that having a PCM with a higher melting temperature in either the upper half of a trans-axial arrangement or the inner layer of a trans-radial configuration could dramatically increase heat transfer coefficients over time. However, in terms of heat transfer coefficients, single layer PCM is more efficient.

4. Conclusions

In this research, the various PCM arrangement methods, including the single- and two-layer arrangements, were taken into consideration. Among the findings reached are

- i. PCM in a single layer configuration shown that RT50 case is 13% faster to completely melt PCM, maintains 10% lower battery temperature and 26% higher heat transfer coefficients compared to RT60 case. This shows that lower melting temperature can reduce the battery temperature for a longer period of time, down to 67°C with RT50 configuration.
- ii. PCM in trans-axial arrangement shown that TA60-50 case is 20% faster to completely melt PCM, maintains 10% lower battery temperature and 16% higher heat transfer coefficients compared to TA50-60 case. This shows with higher melting temperature placed in the upper layer showed lower battery temperature down to 67°C with TA60-50 configuration.
- iii. PCM in trans-radial arrangement shown that TR60-50 case is 10% faster to completely melt PCM, maintains 7% lower battery temperature and average of 7% higher heat transfer coefficients compared to TA50-60 case. This shows with higher melting temperature placed in the inner layer showed lower battery temperature down to 77°C with TR60-50 configuration.
- iv. At 25°C ambient temperature, the single layer arrangement and the trans-axial arrangement perform better compared to trans-radial arrangement.

This study recommends trans-axial arrangements compared to trans-radial and single arrangement for use in controlling battery thermal performance.

Acknowledgement

This research was not funded by any grant.

References

- [1] Panchal, Satyam, Ibrahim Dincer, Martin Agelin-Chaab, Roydon Fraser, and Michael Fowler. "Experimental investigation and simulation of temperature distributions in a 16Ah-LiMnNiCoO₂ battery during rapid discharge rates." *Heat and Mass Transfer* 53 (2017): 937-946. <https://doi.org/10.1007/s00231-016-1870-x>
- [2] Chen, Jingwei, Siyi Kang, E. Jiaqiang, Zhonghua Huang, Kexiang Wei, Bin Zhang, Hao Zhu, Yuanwang Deng, Feng Zhang, and Gaoliang Liao. "Effects of different phase change material thermal management strategies on the cooling performance of the power lithium ion batteries: A review." *Journal of Power Sources* 442 (2019): 227228. <https://doi.org/10.1016/j.jpowsour.2019.227228>
- [3] Kumar, Pradeep, Deepak Chaudhary, Peeyush Varshney, Utkarsh Varshney, Syed Mohd Yahya, and Yasser Rafat. "Critical review on battery thermal management and role of nanomaterial in heat transfer enhancement for electrical vehicle application." *Journal of Energy Storage* 32 (2020): 102003. <https://doi.org/10.1016/j.est.2020.102003>
- [4] Kim, Gi-Heon, and Ahmad Pesaran. "Battery thermal management design modeling." *World Electric Vehicle Journal* 1, no. 1 (2007): 126-133. <https://doi.org/10.3390/wevj1010126>
- [5] Han, Taeyoung, Bahram Khalighi, and Shailendra Kaushik. "Li-ion Battery Thermal Management—Air vs. Liquid Cooling." In *ASTFE Digital Library*. Begel House Inc., 2017. <https://doi.org/10.1615/TFEC2017.fna.017297>
- [6] Keshteli, A. Nematpour, and M. Sheikholeslami. "Nanoparticle enhanced PCM applications for intensification of thermal performance in building: a review." *Journal of Molecular Liquids* 274 (2019): 516-533. <https://doi.org/10.1016/j.molliq.2018.10.151>
- [7] Wang, Jifen, Huaqing Xie, Zhixiong Guo, Lihui Guan, and Yang Li. "Improved thermal properties of paraffin wax by the addition of TiO₂ nanoparticles." *Applied Thermal Engineering* 73, no. 2 (2014): 1541-1547. <https://doi.org/10.1016/j.applthermaleng.2014.05.078>
- [8] Al-Hallaj, Said, Riza Kizilel, Abdul Lateef, Rami Sabbah, Mohammed Farid, and J. Rob Selman. "Passive thermal management using phase change material (PCM) for EV and HEV Li-ion batteries." In *2005 IEEE vehicle power and propulsion conference*, pp. 5-pp. IEEE, 2005.
- [9] Bais, Aditya R., Dattataraya G. Subhedhar, Nishith C. Joshi, and Satyam Panchal. "Numerical investigation on thermal management system for lithium ion battery using phase change material." *Materials Today: Proceedings* 66 (2022): 1726-1733. <https://doi.org/10.1016/j.matpr.2022.05.269>

- [10] Choudhari, V. G., A. S. Dhoble, and T. M. Sathe. "A review on effect of heat generation and various thermal management systems for lithium ion battery used for electric vehicle." *Journal of Energy Storage* 32 (2020): 101729. <https://doi.org/10.1016/j.est.2020.101729>
- [11] Moraga, Nelson O., Jesús P. Xamán, and Ricardo H. Araya. "Cooling Li-ion batteries of racing solar car by using multiple phase change materials." *Applied Thermal Engineering* 108 (2016): 1041-1054. <https://doi.org/10.1016/j.applthermaleng.2016.07.183>
- [12] Nasehi, Ramin, Arghavan Alamatsaz, and Mohammad Reza Salimpour. "Using multi-shell phase change materials layers for cooling a lithium-ion battery." *Thermal Science* 20, no. 2 (2016): 391-403. <https://doi.org/10.2298/TSCI130515033N>
- [13] Jilte, Ravindra, Asif Afzal, and Satyam Panchal. "A novel battery thermal management system using nano-enhanced phase change materials." *Energy* 219 (2021): 119564. <https://doi.org/10.1016/j.energy.2020.119564>
- [14] Yang, Huan, Hengyun Zhang, Yang Sui, and Chun Yang. "Numerical analysis and experimental visualization of phase change material melting process for thermal management of cylindrical power battery." *Applied Thermal Engineering* 128 (2018): 489-499. <https://doi.org/10.1016/j.applthermaleng.2017.09.022>
- [15] Kean, Tung Hao, and Nor Azwadi Che Sidik. "Thermal performance analysis of nanoparticles enhanced phase change material (NEPCM) in cold thermal energy storage (CTES)." *CFD Letters* 11, no. 4 (2019): 79-91.
- [16] Yang, Huan, Hengyun Zhang, Yang Sui, and Chun Yang. "Numerical analysis and experimental visualization of phase change material melting process for thermal management of cylindrical power battery." *Applied Thermal Engineering* 128 (2018): 489-499. <https://doi.org/10.1016/j.applthermaleng.2017.09.022>
- [17] Rao, Zhonghao, Shuangfeng Wang, and Guoqing Zhang. "Simulation and experiment of thermal energy management with phase change material for ageing LiFePO₄ power battery." *Energy Conversion and Management* 52, no. 12 (2011): 3408-3414. <https://doi.org/10.1016/j.enconman.2011.07.009>
- [18] Javani, Nader, I. Dincer, G. F. Naterer, and B. S. Yilbas. "Heat transfer and thermal management with PCMs in a Li-ion battery cell for electric vehicles." *International Journal of Heat and Mass Transfer* 72 (2014): 690-703. <https://doi.org/10.1016/j.ijheatmasstransfer.2013.12.076>
- [19] Palaniappan, P. L., T. T. K. Lokeswar, V. Adhitya, and R. Harish. "CFD Analysis on Thermal Performance of Nanofluids in Electric Vehicle Battery." In *Advances in Thermal Sciences: Select Proceedings of ICFAMMT 2022*, pp. 79-90. Singapore: Springer Nature Singapore, 2022. https://doi.org/10.1007/978-981-19-6470-1_7
- [20] Sankeeth, S. G., S. Kathiresan, J. Harish, D. Srihari, and R. Harish. "Comparison of Heat Transfer Characteristics of Nanofluids for Electric Vehicle Battery Thermal Management." In *Advances in Thermal Sciences: Select Proceedings of ICFAMMT 2022*, pp. 57-68. Singapore: Springer Nature Singapore, 2022. https://doi.org/10.1007/978-981-19-6470-1_5
- [21] Harish, R., Rajesh Nimmagadda, and S. Rajesh Reddy. "Turbulent melting characteristics of hybrid nano-enhanced molten salt phase change material in rectangular enclosure." *Journal of Energy Storage* 54 (2022): 105328. <https://doi.org/10.1016/j.est.2022.105328>
- [22] Raju, Pusapati Laxmi Narasimha, Chalumuru Manas, and Harish Rajan. "Computational modeling of battery thermal energy management system using phase change materials." *International Journal for Simulation and Multidisciplinary Design Optimization* 13 (2022): 1. <https://doi.org/10.1051/smdo/2021034>
- [23] Harish, R. "Buoyancy driven turbulent plume induced by protruding heat source in vented enclosure." *International Journal of Mechanical Sciences* 148 (2018): 209-222. <https://doi.org/10.1016/j.ijmecsci.2018.09.001>
- [24] Ramanathan, Y. Ashwin, G. Anuradha, Harish Rajan, and R. Lakshmi Sriman. "Battery thermal management system using nano enhanced phase change materials." In *IOP Conference Series: Earth and Environmental Science*, vol. 850, no. 1, p. 012031. IOP Publishing, 2021. <https://doi.org/10.1088/1755-1315/850/1/012031>
- [25] Ling, Ziye, Jiajie Chen, Xiaoming Fang, Zhengguo Zhang, Tao Xu, Xuenong Gao, and Shuangfeng Wang. "Experimental and numerical investigation of the application of phase change materials in a simulative power batteries thermal management system." *Applied energy* 121 (2014): 104-113. <https://doi.org/10.1016/j.apenergy.2014.01.075>
- [26] Qin, Peng, Mengran Liao, Danfeng Zhang, Yujun Liu, Jinhua Sun, and Qingsong Wang. "Experimental and numerical study on a novel hybrid battery thermal management system integrated forced-air convection and phase change material." *Energy Conversion and Management* 195 (2019): 1371-1381. <https://doi.org/10.1016/j.enconman.2019.05.084>